Monte Carlo simulation of the acquisition conditions for 177Lu molecular imaging of hepatic tumors

関川, 祐矢

Yuya Sekikawa[1), 2)], Keita Funada[1)], Go Akamatsu[3)] Kazuhiko Himuro[4)], Akihiko Takahashi[5)], Shingo Baba[4)], Masayuki Sasaki[5)]

Title: Monte Carlo simulation of the acquisition conditions for ^{177}Lu molecular imaging of hepatic tumors

Short title: Monte Carlo simulation for ^{177}Lu

1) Department of Health Sciences, Graduate School of Medical Sciences, Kyushu University, 3-1-1 Maidashi, Higashi-ku, Fukuoka 812-8582, Japan.
2) Department of Radiological Technology, Faculty of Fukuoka Medical Technology, Teikyo University, 6-22 Misakimachi, Omuta, Fukuoka 836-8505, Japan
3) National Institute of Radiological Sciences, National Institutes for Quantum and Radiological Science and Technology (NIRS-QST), 4-9-1 Anagawa, Inage-ku, Chiba 263-8555, Japan
4) Division of Radiology, Department of Medical Technology, Kyushu University Hospital, 3-1-1 Maidashi, Higashi-ku, Fukuoka 812-8582, Japan.
5) Department of Health Sciences, Faculty of Medical Sciences, Kyushu University, 3-1-1 Maidashi, Higashi-ku, Fukuoka 812-8582, Japan.

Corresponding author: Akihiko Takahashi
Department of Health Sciences, Faculty of Medical Sciences, Kyushu University,
3-1-1 Maidashi, Higashi-ku, Fukuoka 812-8582, Japan.
E-mail: takahsr@hs.med.kyushu-u.ac.jp
Tel: 092-642-6725
Fax: 092-642-6674

The type of article: Original article

Abstract

Objective: To examine the impact of acquisition time on Lutetium-177 (^{177}Lu) single-photon emission computed tomography (SPECT) images using Monte Carlo simulation. *Methods:* A gamma camera simulation based on the Monte Carlo method was performed to produce SPECT images. The phantom was modeled on a NEMA IEC BODY phantom including six spheres as tumors. After the administration of 7.4 GBq of ^{177}Lu, radioactivity concentrations of the tumor/liver at 6, 24, and 72 h after administration were set to 1.85/0.201, 2.12/0.156, and 1.95/0.117 MBq/mL, respectively. In addition, the radioactivity concentrations of the tumor at 72 h after administration varied by 1/2, 1/4, and 1/8 when comparison was made. Acquisition times examined were 1.2, 1.5, 2, 3, 6, and 12 min. To assess the impact of collimators, SPECT data acquired at 72 h after the administration using six collimators of low-energy high-resolution (LEHR), extended low-energy general-purpose (ELEGP), medium-energy and general-purpose (MEGP-1, MEGP-2, and MEGP-3) and high-energy general-purpose (HEGP) were examined. After prefiltering using a Butterworth filter, projection images were reconstructed using ordered subset expectation maximization. The detected photons were classified into direct rays, scattered rays, penetrating rays, and characteristic X-rays from lead. The image quality was evaluated through visual assessment, and physical assessment of contrast recovery

coefficient (CRC) and contrast-to-noise ratio (CNR). In this study, the CNR threshold for detectability was assumed to be 5.0.

Results: To compare collimators, the highest sensitivity was observed with ELEGP, followed by LEHR and MEGP-1. The highest ratio of direct ray was also observed in ELEGP followed by MEGP-1. In comparison of the radioactivity concentration ratios of tumor/liver, CRC and CNR were significantly decreased with smaller radioactivity concentration ratios. This effect was greater with larger spheres. According to the visual assessment, the acquisition time of 6, 6, and 3 min or longer was required using ELEGP collimator at 6, 24, and 72 h after administration, respectively. Physical assessment based on CNR and CRC also suggested that 6, 6, and 3 min or longer acquisition time was necessary at 6, 24, and 72 h after administration.

Conclusion: ^{177}Lu-SPECT images generated via the Monte Carlo simulation suggested that the recommended acquisition time was 6 min or longer at 6 and 24 h and 3 min or longer at 72 h after administration.

Keywords: Lutetium-177, Theranostics, ^{177}Lu SPECT, Monte Carlo simulation.

Introduction

^{177}Lu-labeled radiopharmaceuticals have been increasingly used for nuclear medicine therapy. ^{177}Lu is a medium-energy β-emitter with a maximum energy of 0.497 MeV with a physical half-life of 6.7 days (1, 2). ^{177}Lu-labeled DOTATE, DOTATOC, and DOTANOC are used for patients with metastatic tumors of neuroendocrine origin (NET) as a peptide receptor radionuclide therapy (PRRT) (3-8). These somatostatin analogs target somatostatin receptors on tumor cells. ^{177}Lu-DOTATE was reported to show better response rate and fewer adverse events than the existing molecular targeted therapy (9). ^{177}Lu-prostate specific membrane antigen is used for metastatic tumors of castration-resistant prostate cancer (10). In addition, the number of ^{177}Lu-labeled compounds has been increasing (11). The therapeutic effect of ^{177}Lu depends on the accumulated radioactivity in the tumor. Furthermore, radiation-induced toxicity also depends on the radiation dose on radiosensitive organs (12-14). Thus, the estimation of absorption dose is extremely important not only to assess the therapeutic effect but also to predict side effects of nuclear medicine therapy.

The kinetics and distribution of ^{177}Lu-labeled radiopharmaceuticals are usually pre-estimated using single-photon emission computed tomography (SPECT) with ^{111}In-labeled radiopharmaceuticals and positron emission tomography with ^{68}Ga-

labeled radiopharmaceuticals before the therapy (15, 16). ^{177}Lu also emits low-energy γ-rays at 208 keV (11.0%) and 113 keV (6.4%), and these photons allow scintigraphy. A scintigraphy with ^{177}Lu-labeled radiopharmaceuticals is expected to be useful for evaluating biodistribution and subsequent dosimetry. Some researchers have already reported the availability of ^{177}Lu SPECT imaging (17-21); however, the appropriate acquisition time for theranostic purpose has not yet been reported.

Although ^{177}Lu-labeled compound has not yet been approved for reimbursement of medical insurance in Japan, an imaging protocol and a therapeutic effect prediction should be established before the clinical use. Our previous studies reported that the Monte Carlo simulation successfully examined the suitable imaging protocol and a therapeutic effect prediction for nuclear medicine therapy (22-25). Optimization of the imaging protocol, such as shortening of the acquisition time, is expected to reduce the patient burden. Therefore, this study aimed to examine the influence of acquisition time on ^{177}Lu SPECT images using the Monte Carlo simulation.

Materials and Methods

Simulation code

The Monte Carlo simulation in this study included in-house codes, MCEP-

SPECT (23), developed based on the gamma camera simulation codes HEXAGON and NAI developed by Tanaka et al. (24). HEXAGON code simulates photon and electron transportation in the phantom and collimator, while NAI code simulates the response of the NAI detector system using results from HEXAGON. The advantage of our simulation codes is the ability to track physical processes and flow in detail, making it easier to understand the internal processes. Specifically, our simulation codes can discriminate scatter components due to high energy gamma rays (23, 24), and detected photons were classified into direct rays ("dir0"), scattered rays ("dir1"), penetrating rays ("indir"), and characteristic X-rays from lead ("Pb-X"). Figure 1 shows simulation setting of SPECT cameras and a phantom based on previous studies (17-21). The collimator and NaI crystal size was 40 × 40 cm. To simulate the effects of backscatter photons from the backward components such as photomultiplier tubes, a glass and an aluminum plate were placed behind NaI.

Six collimators were examined (17-21): low-energy high-resolution (LEHR), extended low-energy general-purpose (ELEGP), three of the medium-energy and general-purpose (MEGP-1, MEGP-2, and MEGP-3), and high-energy general-purpose (HEGP). The characteristics of these six collimators are shown in Table 1.

The computation time was approximately 96 h for 10^{10} decays using an

Intel® Core™ i7 /2.0 GHz central processing unit.

120

Phantom

A NEMA IEC BODY phantom was modeled and consisted of six spheres with diameters of 10, 13, 17, 22, 28, and 37 mm. In this study, the phantom length was 100 mm. The background was assumed to be a healthy liver tissue, whereas the spheres 125 were assumed to be tumors. In previous studies, the ratio between background and tumor has been investigated (26, 27). In this study, we referred to the previous study that provided more detailed data of radioactivity concentrations of liver and tumor (28). Studied tumor-liver ratios were three. After the administration of 7.4 GBq of ^{177}Lu, radioactivity concentrations of the tumor/liver at 6, 24, and 72 h after administration were 130 1.85/0.201 MBq/mL (ratio =9.20), 2.12/0.156 MBq/mL (ratio =13.6), and 1.95/0.117 MBq/mL (ratio =16.7), respectively. In addition, the radioactivity concentrations of the tumor at 72 h after administration varied by 1/2, 1/4, and 1/8 when compared (the radioactivity concentrations of the tumor/liver were 0.974/0.117 MBq/mL [ratio = 8.32], 0.487/0.117 MBq/mL [ratio = 4.16], and 0.244/0.117 MBq/mL [ratio = 2.08]).

135

Data acquisition

The main energy window was 187–229 keV (208 keV ± 10 %), with 208 keV gamma ray as most frequent (10.41 %) among 6 gamma rays emitted from ^{177}Lu (Table 2). The number of projection was 96 per 360° for two detectors. The rotation radius was 230 mm. Projection images were 128 × 128 pixels for the field of view of 40 × 40 cm; therefore, the pixel size was 3.13 × 3.13 mm. Data acquisition was performed at 6, 24, and 72 h post-injection. Acquisition times were for 1.2, 1.5, 2, 3, 6, and 12 min. To compare collimators, SPECT data were acquired at 72 h after the administration for 1.2 min.

Image reconstruction

SPECT images were produced using the Prominence Processor™ version 3.1 (Nihon Medi-Physics Co., Ltd., Osaka, Japan). Reconstruction algorithms and various corrections have been studied in previous studies and referred to in this study (17-21). Projection images were pre-filtered using a Butterworth filter (cut-off frequency: 0.50 cycle/cm, order: 8). Projection images were reconstructed using ordered subset expectation maximization method (OSEM) with 8 iterations and 6 subsets. Reconstructed images were then corrected by attenuation correction using the Chang method (0.13/cm). Scatter correction was not performed.

155

Image assessment

The regions of interest (ROIs) were placed on all spheres at the center slice of phantom (Figure 2). The diameter of sphere ROIs was defined as the diameter of each sphere. Twelve background ROIs with 37 cm diameter were placed at the periphery. The
160 value of each ROIs was expressed as the mean count per pixel.

For the visual assessment of image quality, SPECT images were evaluated using the detectability of 10-mm sphere and background uniformity by a board-certified nuclear medicine physician and two radiological technologists. The detectability of 10-mm sphere was classified into a 5-score scale: 1, definitely absent; 2, probably absent; 3,
165 equivocal; 4, probably present; and 5, definitely present (29, 30). The background uniformity was also classified into a 5-score scale: 1, very poor; 2, poor; 3, fair; 4, good; and 5, very good. Images were randomly evaluated without any information about the acquisition condition and reconstruction parameters. The scores of the three observers were averaged. The total score of 10-mm sphere detectability and background uniformity
170 of >6.0 was considered appropriate. The visual assessment of the image at 72 h after administration was performed only for the case of the ratio =16.7.

The image quality was physically evaluated using contrast recovery

coefficient (CRC) and contrast-to-noise ratios (CNR). CRC is the ratio of the count ratio of images to the true radioactivity ratio that indicates its accuracy. CNR is the ratio of the signal of hot spheres to the standard deviation of the background activity. The CNR is a detectable index on how easily is the sphere detected. In this study, the detectability threshold was assumed to be CNR = 5 according to previous studies (31, 32). CRC and CNR are defined using the following equation:

$$\mathrm{CRC}_{H,j} = \frac{{C_{H,j}}/{C_B} - 1}{{a_H}/{a_B} - 1} \times 100 \quad (1)$$

$$\mathrm{CNR} = \frac{C_{H,j} - C_B}{SD_{B,mean}} \quad (2)$$

where the subscript *"H*" denotes the hot sphere, "*B*" denotes the background, *j* is the size of the sphere, $C_{H,j}$ is the count of the hot sphere *j*, C_B is the average count of 12 background ROIs, $SD_{B,\mathrm{mean}}$ is the mean standard deviation of count in 12 background ROIs, a_H is the true radioactivity concentration of the hot sphere and a_B is the true radioactivity concentration of the background. The image assessment of the comparison of radioactivity concentration ratio was performed by physical assessment only.

Results

Collimator comparison

Figure 3 shows SPECT images using six collimators at 72 h after administration. A 13-mm sphere was visible in all collimators. A 10-mm sphere was visible in LEHR, ELEGP, MEGP-1, and MEGP-3, but not in MEGP-2 and HEGP. The background uniformity was almost equivalent among collimators. The LEHR image showed a relatively noisier background and more artifacts outside the phantom.

Figure 4 shows CRC and CNR of different collimators. Neither CRC nor CNR of 10-mm sphere were not measured in HEGP. In other five collimators, both CRC and CNR of all spheres were not significantly different.

Figure 5 shows the detector sensitivity and proportion of detected photons. The detector sensitivity in LEHR, ELEGP, MEGP-1, MEGP-2, MEGP-3, and HEGP was 3.99, 4.74, 3.82, 2.01, 3.06, and 2.27 cps/MBq, respectively. The Pb-X was not measurable in all collimators. The highest sensitivity was observed in ELEGP, followed by LEHR and MEGP-1. The highest “dir0” was also observed in ELEGP, followed by MEGP-1. The LEHR showed the second highest sensitivity, whereas the “indir” component was 53 %. Both MEGP-2 and HEGP showed relatively low sensitivity.

Comparison of the radioactivity concentration ratio of tumor/liver

Figure 6 shows CRC and CNR in each sphere size with different radioactivity concentrations in the liver (that is, with different tumor/liver radioactivity concentration ratios). Both CRC and CNR were high with larger sphere in any of the radioactivity concentration. CRC and CNR significantly decreased with smaller radioactivity concentrations. This effect was greater with larger sphere size.

Comparison of the acquisition condition

Figure 7 shows simulated ^{177}Lu SPECT images using ELEGP collimator with different acquisition time and time after administration. The longer the acquisition time, the better the background homogeneity. The visibility of 10-mm sphere improved by long acquisition time. The contrast between the sphere and the background tended to increase in relation to the long acquisition time and the time after administration.

Results of visual assessment are shown in Table 3. Both scores of a 10-mm sphere and background were generally high in the long acquisition time at any time after administration. At 6 and 24 h after administration, the total score exceeded six when the acquisition time was >6 min. At 72 h after administration, the acquisition time of >3 min was required to exceed total score of six.

Figure 8 shows CRC in relation to the acquisition time and time after

administration. The CRC was high in large sphere and was not significantly different for any acquisition time and at any time after administration. The CRC fluctuated in short acquisition time. Figure 9 shows CNR in relation to the acquisition time and time after administration. The CNR increased with the long acquisition time at any time after administration. The CNR at 24 and 72 h after administration was higher than that at 6 h. The CNR of 13–37-mm spheres were >5 for any acquisition time and time after administration. The CNR of 10-mm spheres were >5 in ≥6 min acquisition time at 6 and 24 h after administration. The CNR of 10-mm sphere was >5 in ≥1.5 min acquisition time at 72 h after administration. However, the CNR was exceptionally higher than the exceptions of 2 and 3 min. The acquisition time of 6, 6, and 3 min or longer was comprehensively considered to be required at 6, 24, and 72 h after administration.

Discussion

In this study, the influence of acquisition time on ^{177}Lu-SPECT images generated by the Monte Carlo simulation was examined using visual and physical evaluations. The recommended collimator for ^{177}Lu-SPECT was ELEGP followed by MEGP-1. In ^{177}Lu-SPECT using ELEGP collimator, CNRs of SPECT images improved as the acquisition time at any time after administration became long. The recommended

245 acquisition time was ≥6 min at 6 and 24 h, and ≥3 min at 72 h after administration.

The most appropriate collimator among 6 collimators examined was considered ELEGP, followed by MEGP-1, based on the visual and physical evaluation and sensitivity analysis. A previous study examined LEHR, LEGP, and MEGP to determine an optimal condition for a dosimetry of ^{177}Lu imaging (33). The % difference 250 of sphere-to-background ratio between the true radioactivity concentration and count in images was used as an index. Their results showed that %difference was the smallest in MEGP (-10.9 ± 9.7%), followed by LEGP (-44.1 ± 7.5%) and LEHR (-66.3 ± 13.2%). They suggested that the MEGP was an optimal collimator and considered septal penetration of primary imaging photons that deteriorate the LEGP and LEHR results. This 255 is consistent with our study demonstrating that the largest penetrating photon "indir" was observed in LEHR. Furthermore, although neither CRC nor CNR did not show significant difference among collimators in this study, the detector sensitivity of the direct photon "dir0" was the largest in ELEGP, followed by MEGP-1. ELEGP is a vender specific collimator, although its structural feature is similar to that of MEGP-1. Because ELEGP 260 is not generally available, MEGP-1 is considered as another candidate for ^{177}Lu-SPECT. In a previous study, the system sensitivity of low-energy collimators was higher than that of medium or high-energy collimators (34). However, relatively large ratio of "indir"

deteriorates image quality of LEHR. They suggested that medium-energy collimators were preferable for ^{177}Lu imaging because of their lower septal penetration of the high-energy photons emitted by ^{177}Lu. Although high-energy collimators had slightly better sensitivity for 208 keV photons than medium-energy collimators, an inferior spatial resolution of high-energy collimator due to their wider holes could be a problem in clinical use (34). In clinical practice, medium-energy collimators have been widely used (7, 12, 17, 18, 26, 35, 36). However, the largely different characteristics among MEGP-1, MEGP-2, and MEGP-3 should be considered.

Both CRC and CNR were high with larger sphere size and radioactivity concentration. Previous studies have shown that tumor size and ratio of tumor to background increases for NET, with high malignancy (26). Therefore, based on the results of CRC and CNR in this study, the time required for image acquisition should be set longer than 12 minutes in order to improve the image quality for low-grade tumors and tumors with low accumulation less than 1/4 of the set radioactivity concentration (0.487 MBq).

The optimal acquisition time was considered to be 6, 6, and 3 min or longer at 6, 24, and 72 h after administration, respectively. Some previous clinical studies have acquired ^{177}Lu-SPECT data with relatively long acquisition time for 15–32 min (7, 12,

26, 35, 36). Conversely, some studies acquired data with relatively short acquisition time for 8–12 min (17, 18). These studies demonstrated that the acquired SPECT data showed sufficient quality for the quantification of ^{177}Lu activity distribution. Although a longer acquisition provides better image quality and accurate quantification, it also increases patient burden. Furthermore, quantification for theragnostic purpose sometimes requires whole-body SPECT with multiple bed positions. The acquisition time in our study is shorter than that of previous studies and was 6, 6, and 3 min or longer at 6, 24, and 72 h after administration, respectively. Visual evaluation showed the sufficient image quality with these acquisition time. CRC was stable and did not improve any more using longer than these acquisition time. Although the CNR increased with the long acquisition time, the CNR was >5 for any acquisition time. Some previous studies adopted resolution recovery algorithm for image reconstruction (37-39). It is expected to improve the quantitative accuracy of small lesion, although it is also known to result overestimation (40). Further examination is required to clarify the influence of resolution recovery on the quantitative accuracy.

This study has some limitations. First, the Monte Carlo simulation was performed using an in-house hand-made code. Data acquisition was restricted to circular orbit and step-and-shoot mode. Different acquisition protocols should be further

examined. Second, in this study, the background was the liver, and we did not compare tumors to other organs. Therefore, background tumor ratios using other organ data should also be considered. Third, it is expected that more detailed image quality data can be obtained by further refining the time interval settings for the acquisition time. Fourth, scatter correction was not performed in this study because it reduces the counts used for image reconstruction. Previous studies reconstructed SPECT images by using OSEM algorithm with all of attenuation correction, scatter correction and resolution recovery (17-21, 34), and the usefulness of scatter correction for quantitative accuracy was reported (18). Thus, the scatter correction should be further examined with sufficient count acquisition. Finally, the dead time correction was not required for this simulation study. The usefulness of the dead time correction should be further required in case of clinical situation.

Conclusions

In conclusion, the Monte Carlo simulation generated ^{177}Lu-SPECT images and recommended ELEGP as an optimal collimator, followed by MEGP-1. ^{177}Lu-SPECT images using ELEGP collimator improved in relation to long acquisition time at any time after administration. The recommended acquisition time was ≥6 min at 6 and 24 h and ≥3

min at 72 h after administration.

References

1. Kellett MA. ^{177}Lu: DDEP Assessment of the decay scheme for an emerging radiopharmaceutical. Appl Radiat Isot. 2016; 109: 129-32.
2. Kossert K, Näle OJ, Ott O, Dersch R. Activity determination and nuclear decay data of ^{177}Lu. 2012; 70: 2215-21.
3. Sanders JC, Kuwert T, Hornegger J, Ritt P. Quantitative SPECT/CT Imaging of ^{177}Lu with In Vivo Validation in Patients Undergoing Peptide Receptor Radionuclide Therapy. Mol Imaging Biol. 2015; 17: 585-93.
4. Gleisner KS, Brolin G, Sundlöv A, Mjekiqi E, Östlund K, Tennvall J, et al. Long-Term Retention of ^{177}Lu/^{177m}Lu-DOTATATE in Patients Investigated by g-Spectrometry and g-Camera Imaging. J Nucl Med. 2016; 56: 976-84.
5. Rudisile S, Gosewisch A, Wenter V, Unterrainer M, Böning G, Gildehaus FJ, et al. Salvage PRRT with ^{177}Lu-DOTA-octreotate in extensively pretreated patients with metastatic neuroendocrine tumor (NET): dosimetry, toxicity, efficacy, and survival. BMC Cancer. 2019; 19: 788. doi: 10.1186/s12885-019-6000-y.
6. Satapathy S, Mittal B. ^{177}Lu-DOTATATE peptide receptor radionuclide therapy versus Everolimus in advanced pancreatic neuroendocrine tumors: a systematic review and meta-analysis. Nucl Med Commun. 2019; 40(12): 1195-203.

7. Garkavij M, Nickel M, Gleisner KS, Ljungberg M, Ohlsson T, Wingårdh K, et al. ^{177}Lu-[DOTA0, Tyr3] Octreotate Therapy in Patients With Disseminated Neuroendocrine Tumors: Analysis of Dosimetry With Impact on Future Therapeutic Strategy. Cancer. 2010; 116: 1084-92.

8. Maaß C, Sachs JP, Hardiansyah D, Mottaghy FM, Kletting P, Glatting G. Dependence of treatment planning accuracy in peptide receptor radionuclide therapy on the sampling schedule. Eur J Nucl Med Mol Imaging. 2016; 6: 30. doi: 10.1186/s13550-016-0185-8.

9. Melis M, Swart JD, Visser MD, Berndsen SC, Koelewijin S, Valkema R, et al. Dynamic and Static Small-Animal SPECT in Rats for Monitoring Renal Function After ^{177}Lu-Labeled Tyr3-Octreotate Radionuclide Therapy. J Nucl Med. 2010; 51: 1962–68.

10. Baum RP, Kulkarni HR, Schuchardt C, Singh A, Wirtz M, Wiessalla S, et al. Lutetium-177 PSMA Radioligand Therapy of Metastatic Castration-Resistant Prostate Cancer: Safety and Efficacy. J Nucl Med. 2016; doi: 10.2967/jnumed.115.168443.

11. Khawar A, Eppard E, Roesch F, Ahmadzadehfar H, Kürpig S, Meisenheimer M, et al. Biodistribution and post-therapy dosimetric analysis of [^{177}Lu]Lu-

DOTA^{ZOL} in patients with osteoblastic metastases: first results. EJNMMI Res, 2019; 9: 102. doi: 10.1186/s13550-019-0566-x.

12. Chicheportiche A, Haim SB, Glasberg SG, Oleinikov K, Meirovitz A, et al. Dosimetry after peptide receptor radionuclide therapy: impact of reduced number of post-treatment studies on absorbed dose calculation and on patient management. Eur J Nucl Med Mol Imaging. 2020; 7: 5. doi: 10.1186/s40658-020-0273-8.

13. Vallabhajosula S, Goldsmith SJ, Hamacher KA, Kostakoglu L, Konishi S, Gross DJ, et al. Prediction of myelotoxicity based on bone marrow radiation-absorbed dose: radioimmunotherapy studies using ^{90}Y- and ^{177}Lu-labeled J591 antibodies specific for prostate specific membrane antigen. J Nucl Med. 2005; 46: 850-58.

14. Zaknun JJ, Bodei L, Mueller-Brand J, Pavel ME, Baum RP, Hörsch D, et al. The joint IAEA, EANM, and SNMMI practical guidance on peptide receptor radionuclide therapy (PRRNT) in neuroendocrine tumours. Eur J Nucl Med Mol Imaging. 2013; 40: 800-816.

15. Hijnen NM, Vries AD, Nicolay K, Grüll H. Dual-isotope ^{111}In/^{177}Lu SPECT imaging as a tool in molecular imaging tracer design. Contrast Media Mol Imaging. 2012; 7: 214-222.

16. Meyer JV, Magill S, Lee J, Umetsu S, Flavell R. Detection of Metastatic Meningioma to the Liver Using ^{68}Ga-DOTA-Octreotate PET/CT. Clin Nucl Med. 2018; 43(9): 338-40.

17. Beauregard JM, Hofman MS, Pereira JM, Eu P, Hicks RJ. Quantitative ^{177}Lu SPECT (QSPECT) imaging using a commercially available SPECT/CT system. Cancer Imaging. 2011; 11: 56-66.

18. Hippeläinen E, Tenhunen M, Mäenpää H, Sohlberg A. Quantitative accuracy of ^{177}Lu SPECT reconstruction using different compensation methods: phantom and patient studies. Eur J Nucl Med Mol Imaging. 2016; 6: 16. doi: 10.1186/s13550-016-0172-0.

19. Uribe CF, Esquinas PL, Tanguay J, Gonzalez M, Gaudin E, Beauregard JM, et al. Accuracy of ^{177}Lu activity quantification in SPECT imaging: a phantom study. Eur J Nucl Med Mol Imaging. 2017; 4: 2. doi: 10.1186/s40658-016-0170-3.

20. Shcherbinin S, Bilska HP, Celler A, Birkenfeld B. Quantitative SPECT/CT reconstruction for ^{177}Lu and ^{177}Lu/^{90}Y targeted radionuclide therapies. Phys Med Biol. 2012; 57: 5733-47.

21. D'Arienzo M, Cazzato M, Cozzella ML, Cox M, D'Andra M, Fazio A, et al. Gamma camera calibration and validation for quantitative SPECT imaging with

^{177}Lu. Appl Radiation and Isotopes. 2016; 112: 156-64.

22. Uehara S. The development of a Monte Carlo code simulating electron-photon showers and its assessment by various transport benchmarks. Nucl Insrum Methods. Phys Res B. 1986; 14: 559-70.

23. Takahashi A, Himuro K, Yamashita Y, Komiya I, Baba S, Sasaki M. Monte Carlo simulation of PET and SPECT imaging of ^{90}Y. Med Phys. 2015; 42(4): 1926-35.

24. Tanaka M, Uehara S, Kojima A, Matsumoto M. Monte Carlo simulation of energy spectra for ^{123}I imaging. Phys. Med. Biol. 2007; 52: 4409-25.

25. Takahashi A, Miwa K, Sasaki M, Baba S. A Monte Carlo study on ^{223}Ra imaging for unsealed radionuclide therapy. Med Phys. 2016; 43(6): 2965-74.

26. Kälkner KM, Janson ET, Nilsson S, Carlsson S, Öberg K, Westrin JE et al. Somatostatin Receptor Scintigraphy in Patients with Carcinoid Tumors: Comparison between Radioligand Uptake and Tumor Markers. Cancer Res. 1995; 55: 5801-04.

27. Kim Y, Yoo C, Oh SJ, Lee SJ, Kang J, Hwang HS et al. Tumour-to-liver ratio determined by [68Ga] Ga-DOTA-TOC PET/CT as a prognostic factor of lanreotide efficacy for patients with well-differentiated gastroenteropancreatic-neuroendocrine tumours. EJNMMI Res. 2020; 10: 63. doi: 10.1186/s13550-020-

00651-z.

28. Brolin G, Gustafsson J, Ljungberg M, Gleisner KS. Pharmacokinetic digital phantoms for accuracy assessment of image-based dosimetry in ^{177}Lu-DOTATATE peptide receptor radionuclide therapy. Phys Med Biol. 2015; 60: 6131-49.

29. Taniguchi T, Akamatsu G, Kasahara Y, Mitsumoto K, Baba S, Tsutsui Y, et al. Improvement in PET/CT image quality in overweight patients with PSF and TOF. Ann Nucl Med. 2015; 29: 71-77.

30. Hashimoto N, Morita K, Tsutsui Y, Himuro K, Baba S, Sasaki M. Time-of-Flight Information Improved the Detectability of Subcentimeter Spheres Using a Clinical PET/CT Scanner. J Nucl Med Technol. 2018; 46(3): 268-73.

31. Rose A. Vision - Human and Electronic. Plenum Press. 1973.

32. Cherry SR, Sorenson JA, Phelps ME. Physics in Nuclear Medicine. 3rd ed. Pennsylvania. Elsevier. 2003.

33. de Nijsa R, Lagerburg V, Klausena TL, Holm S. Improving quantitative dosimetry in 177Lu-DOTATATE SPECT by energy window-based scatter corrections. Nucl Med Commun. 2014; 35: 522-33.

34. Ljungberg M, Celler A, Konijnenberg MW, Eckerman KF, Dewaraja YK,

Sjögreen-Gleisner K. MIRD Pamphlet No. 26: Joint EANM/MIRD Guidelines for Quantitative 177Lu SPECT Applied for Dosimetry of Radiopharmaceutical Therapy. J Nucl Med. 2016; 57: 151-62.

35. Garske U, Sandström M, Johansson S, Sundin A, Granberg D, Eriksson B, et al. Minor changes in effective half-life during fractionated ^{177}Lu-Octreotate therapy. Acta Oncol. 2012; 51: 86-96.

36. Guerriero F, Ferrari ME, Botta F, Fioroni F, Grassi E, Versari A, et al. Kidney Dosimetry in 177Lu and 90Y Peptide Receptor Radionuclide Therapy: Influence of Image Timing, Time-Activity Integration Method, and Risk Factors. Bio Res Int. 2013. doi: 10.1155/2013/935351.

37. Bai B, Esser PD. The effect of edge artifacts on quantification of positron emission tomography. In: IEEE nuclear science symposium and medical imaging conference (NSS/MIC). 2010; 2263-6.

38. Tran-Gia J, Lassmann M. Characterization of Noise and Resolution for Quantitative ^{177}Lu SPECT/CT with xSPECT Quant. J Nucl Med. 2019; 60: 50-59.

39. Daou D, Pointurier I, Coaguila C, Vilain D, Benada AW, Lebtahi R, et al. Performance of OSEM and Depth-Dependent Resolution Recovery Algorithms

for the Evaluation of Global Left Ventricular Function in ^{201}Tl Gated Myocardial Perfusion SPECT. J Nucl Med. 2003; 44: 155-162.

40. Kidera D, Kihara K, Akamatsu G, Mikasa S, Taniguchi T, Tsutsui Y, et al. The edge artifact in the point-spread function-based PET reconstruction at different sphere-to-background ratios of radioactivity. Ann Nucl Med. 2016; 30: 97-103.

Figure Legends

Figure 1. Setup for the simulation of single-photon emission computed tomography (SPECT) imaging. The phantom was modeled on a NEMA IEC BODY phantom. Spheres were installed in the phantom with diameters of 10, 13, 17, 22, 28, and 37 mm.

Figure 2. Setting of regions of interest (ROI). ROIs of bold black circle is set on the SPECT image of ^{177}Lu. (a) hot spheres, (b) the background ROI.

Figure 3. SPECT images using low-energy high-resolution (LEHR), extended low-energy general-purpose (ELEGP), medium-energy and general-purpose (MEGP-1, MEGP-2, MEGP-3), and high-energy general-purpose (HEGP). A 10-mm sphere was visible in LEHR, ELEGP, MEGP-1, and MEGP-3, but not in MEGP-2, and HEGP. The image with LEHR showed a relatively noisier background and adequate artifacts outside the phantom.

Figure 4. Physical evaluation in different collimators. (a) Contrast recovery coefficient (CRC) and (b) contrast-to-noise ratio (CNR). The CRC and CNR of all acquisition conditions were slightly different among collimators.

Figure 5. The detector sensitivity in different collimators. The highest sensitivity was observed with ELEGP, followed by LEHR and MEGP-1. The highest “dir0” was also observed in ELEGP, followed by MEGP-1. Both of MEGP-2 and HEGP showed a relatively low sensitivity.

Figure 6. Simulated images were acquired for 12 min at 72 h after administration. The collimator was ELEGP. Both CRC and CNR decreased at lower radioactivity concentration ratio.

Figure 7. The simulated ^{177}Lu SPECT images in different acquisition times. The longer the acquisition time, the better the homogeneity of the background. The visibility of 10-mm sphere improved with long acquisition time.

Figure 8. The CRC in different acquisition times. The CRC at (a) 6, (b) 24, and (c) 72 h. The CRC was not significantly different for any acquisition time and time after administration. The CRC fluctuated in a short acquisition time.

Figure 9. The CNR in different acquisition time. The CNR at (a) 6, (b) 24, and (c) 72 h. The CNR at 24 and 72 h after administration were higher than that at 6 h. The CNR of 10-mm spheres were >5 in ≥6 min acquisition time at 6 and 24 h after administration and in ≥1.5 min acquisition time at 72 h after administration.

Table 1. Characteristics of six collimators.

Collimator	Hole diameter (cm)	Septal thickness (cm)	Hole length (cm)
LEHR	0.150	0.020	3.500
ELEGP	0.250	0.040	4.000
MEGP-1	0.294	0.114	4.064
MEGP-2	0.300	0.105	5.800
MEGP-3	0.340	0.086	5.840
HEGP	0.400	0.180	6.600

low-energy high-resolution, LEHR; extended low-energy general-purpose, ELEGP; medium-energy and general-purpose, MEGP-1, MEGP-2, and MEGP-3; high-energy general-purpose, HEGP.

Table 2. The energies and probability of β and γ emissions from the decay of Lutetium-177

Energy (keV)	Probability (%)	Radiation
175.9	11.52	β^-
247.5	0.02	β^-
384.3	9.01	β^-
497.2	79.44	β^-
71.6	0.16	γ (Hf)
112.9	6.22	γ (Hf)
136.7	0.05	γ (Hf)
208.4	10.41	γ (Hf)
249.7	0.21	γ (Hf)
321.3	0.20	γ (Hf)

490

Table 3. Visual assessment of Lutetium-177 single-photon emission computed tomography images. The radioactivity concentration ratio for 72 h is 16.7.

Time after administration (hours)	Acquisition time (minutes)	Score obtained by visual assessment		
		10-mm sphere	Background	Total
6	1.2	1.0	2.3	3.3
	1.5	1.7	2.3	4.0
	2	1.7	2.3	4.0
	3	1.3	3.3	4.7
	6	2.3	4.3	6.7
	12	3.0	4.7	7.7
24	1.2	1.0	2.7	3.7
	1.5	1.7	2.3	4.0
	2	2.0	3.3	5.3
	3	2.0	3.7	5.7
	6	2.0	4.7	6.7
	12	3.0	4.7	7.7
72	1.2	1.0	2.3	3.3
	1.5	3.0	2.0	5.0
	2	2.0	3.0	5.0
	3	3.0	4.0	7.0
	6	2.7	4.3	7.0
	12	3.0	4.7	7.7

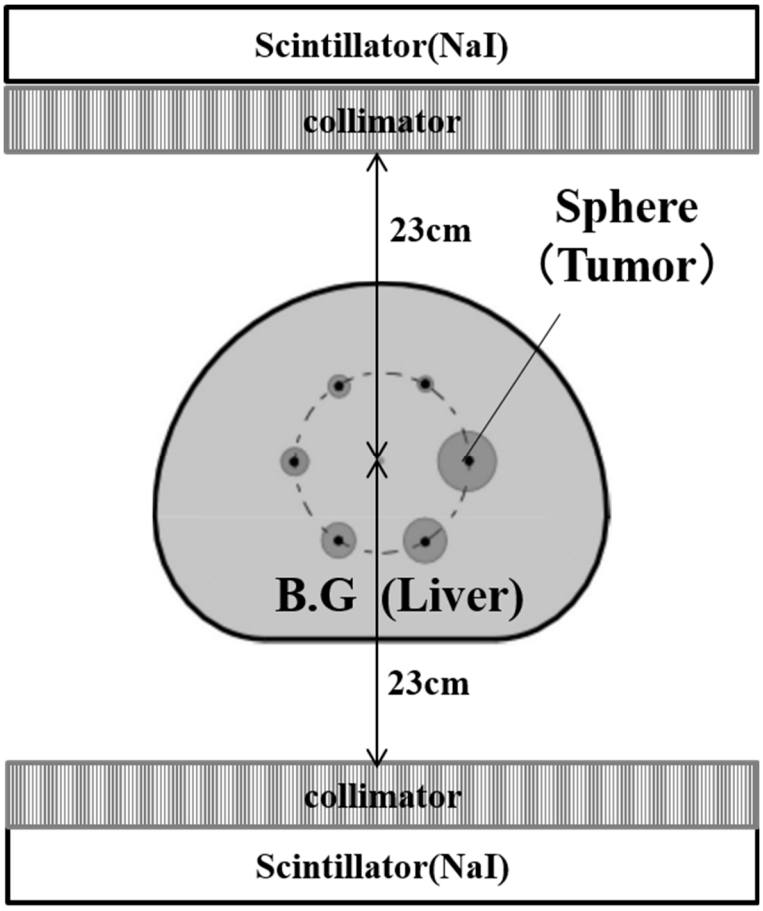
Scintillator(NaI)
collimator
23cm
Sphere
(Tumor)
B.G (Liver)
23cm
collimator
Scintillator(NaI)

Figure 1

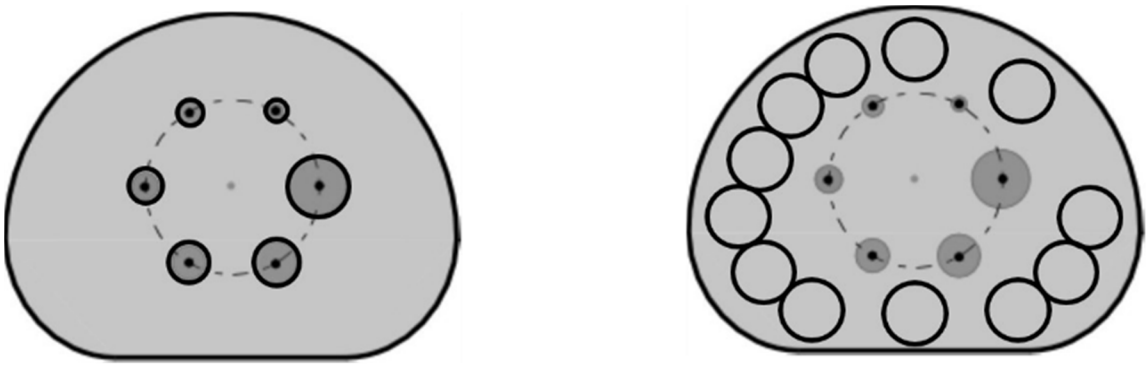

(a) (b)

Figure 2

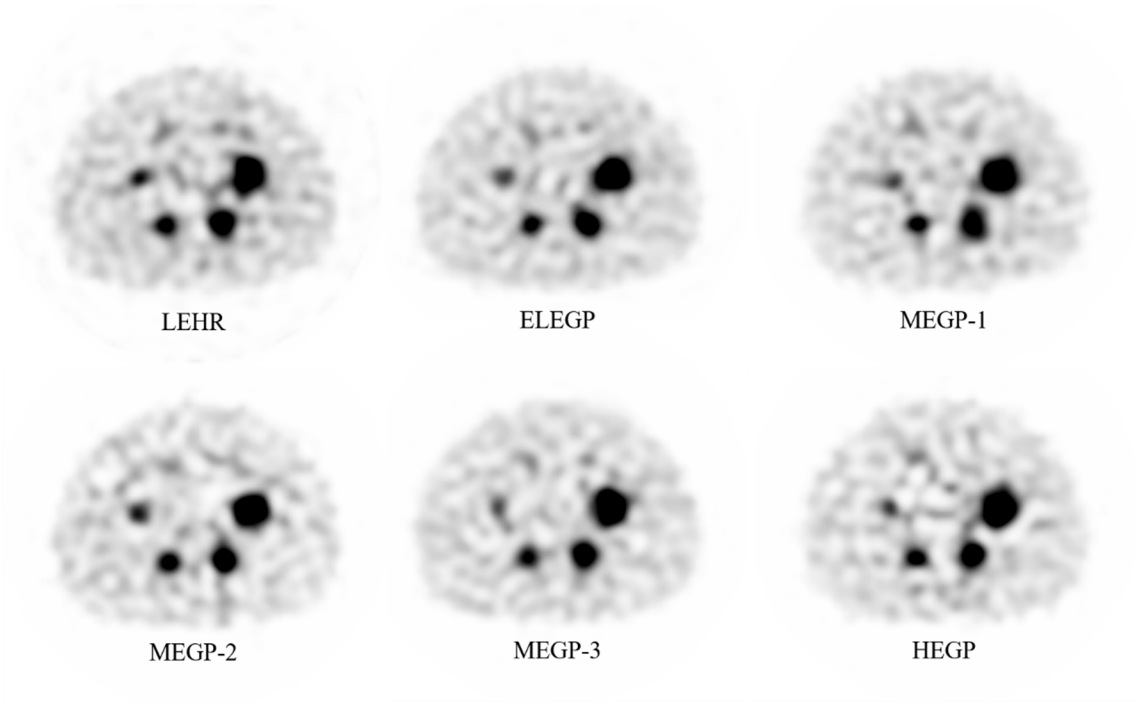

Figure 3

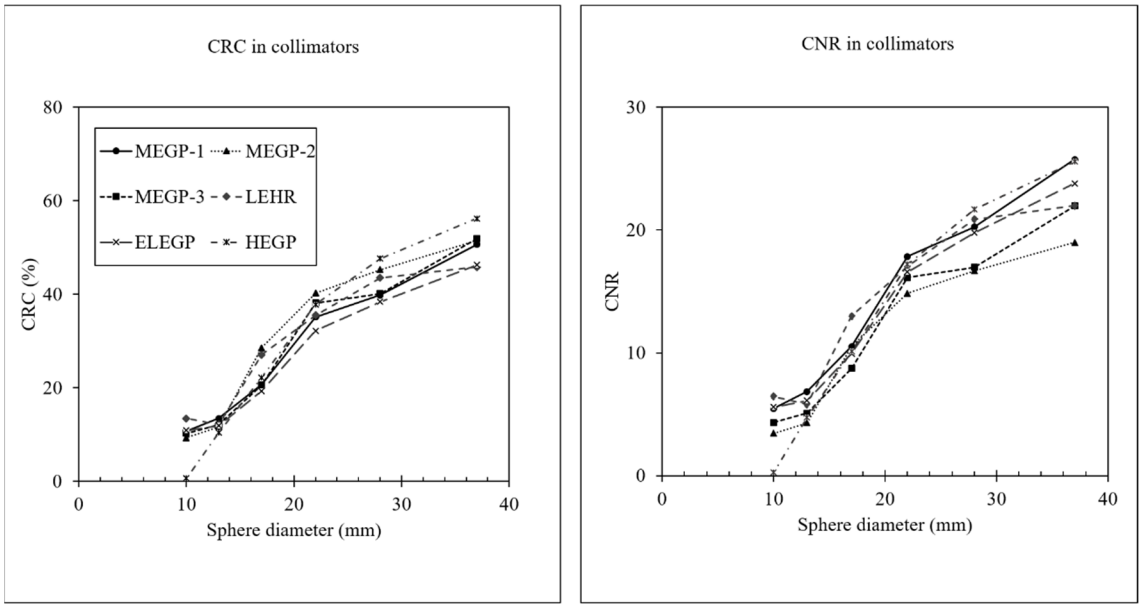
CRC in collimators
CRC (%)
Sphere diameter (mm)
MEGP-1
MEGP-2
MEGP-3
LEHR
ELEGP
HEGP
CNR in collimators
CNR
Sphere diameter (mm)

(a) (b)

Figure 4

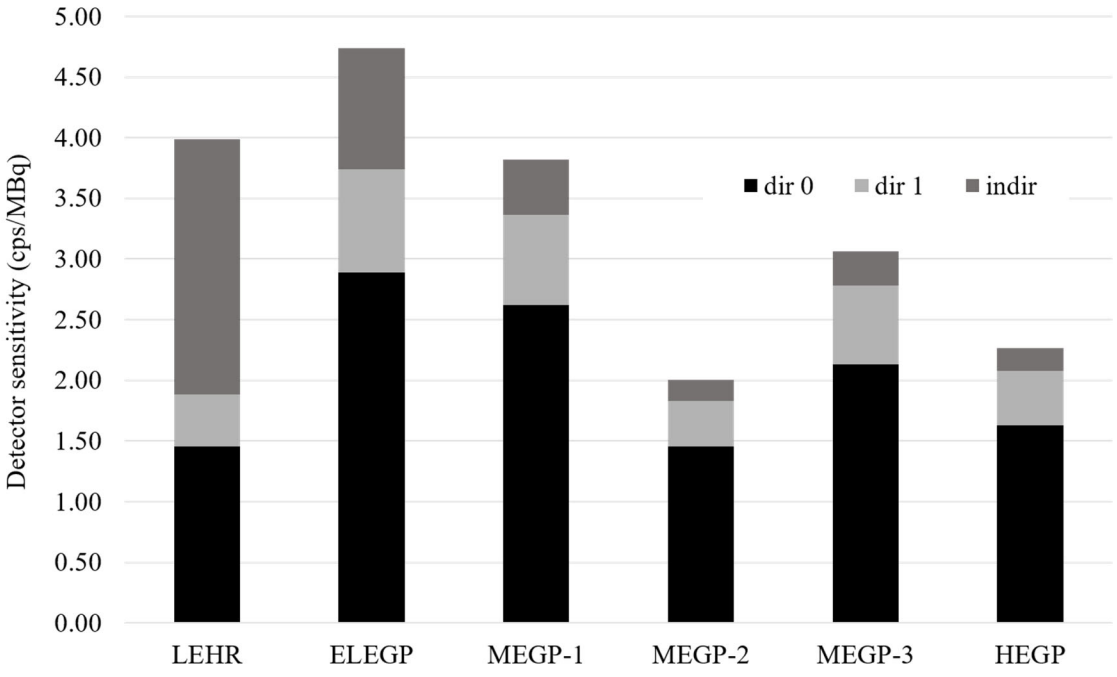
5.00
4.50
4.00
3.50
3.00
2.50
2.00
1.50
1.00
0.50
0.00
Detector sensitivity (cps/MBq)
dir 0
dir 1
indir
LEHR
ELEGP
MEGP-1
MEGP-2
MEGP-3
HEGP

Figure 5

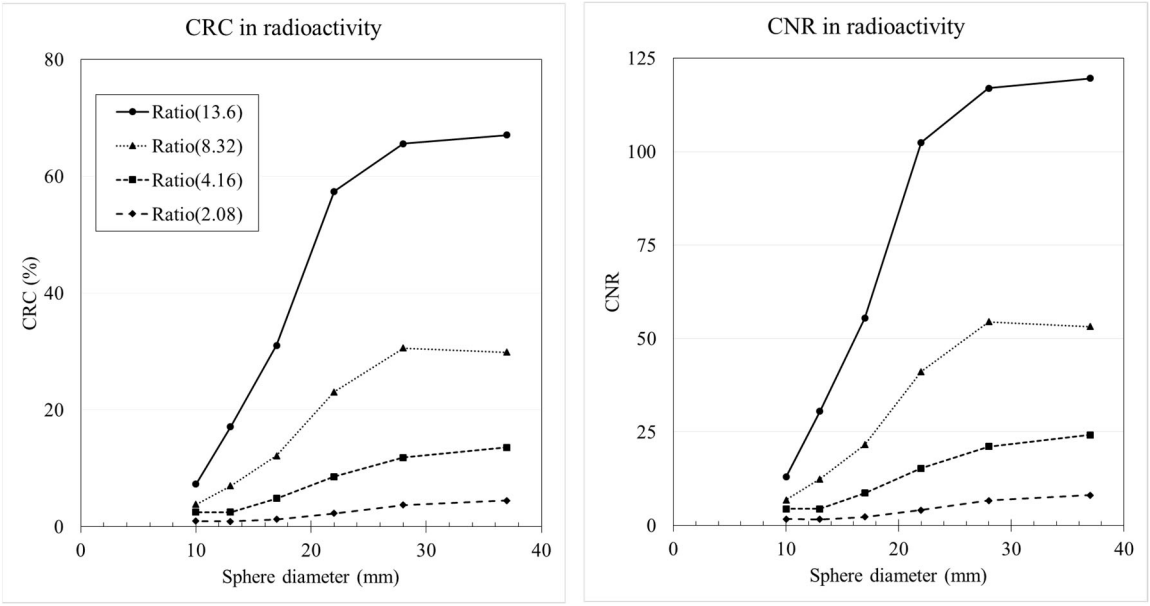
CRC in radioactivity
Ratio(13.6)
Ratio(8.32)
Ratio(4.16)
Ratio(2.08)
CRC (%)
Sphere diameter (mm)
CNR in radioactivity
CNR
Sphere diameter (mm)

(a) (b)

Figure 6

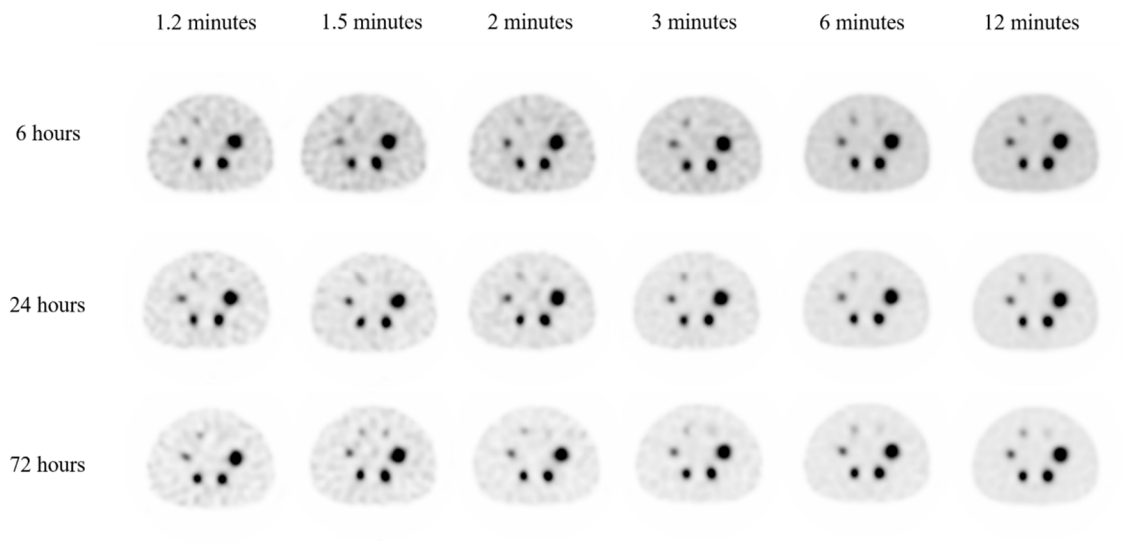
1.2 minutes
1.5 minutes
2 minutes
3 minutes
6 minutes
12 minutes
6 hours
24 hours
72 hours

Figure 7

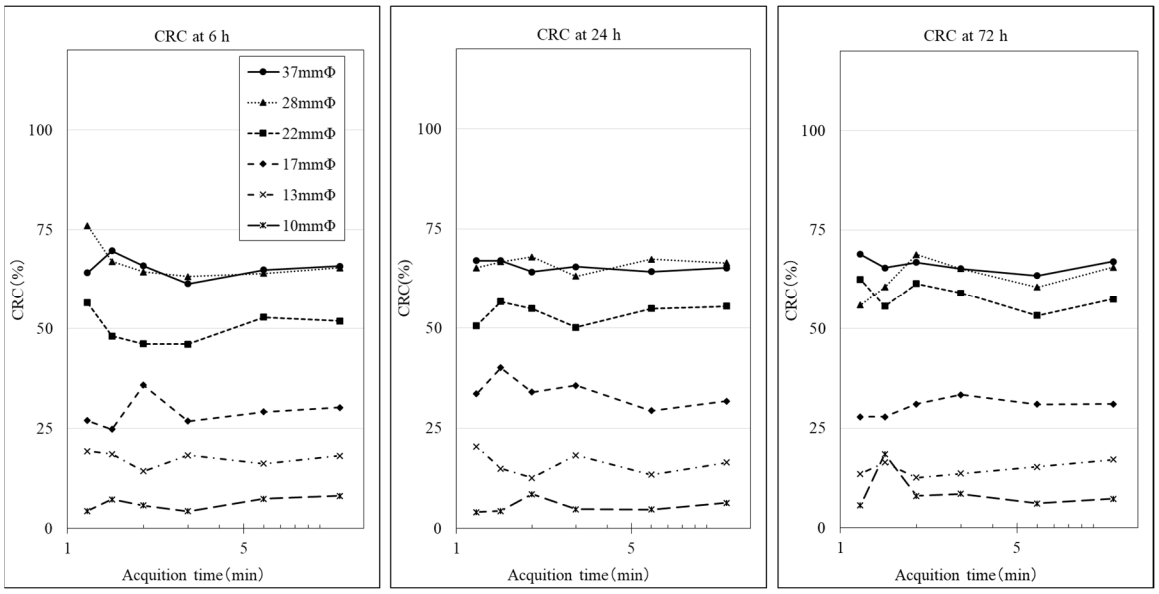
CRC at 6 h
CRC at 24 h
CRC at 72 h
37mmΦ
28mmΦ
22mmΦ
17mmΦ
13mmΦ
10mmΦ
CRC(%)
Acquition time(min)
0
25
50
75
100
1
5

(a) (b) (c)

Figure 8

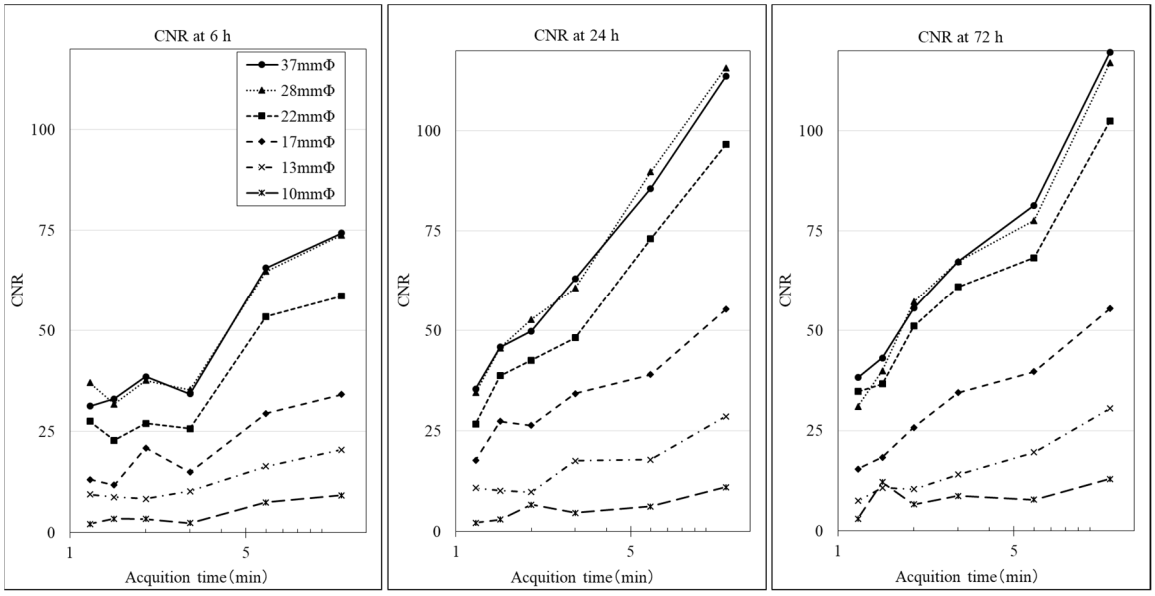
CNR at 6 h
CNR at 24 h
CNR at 72 h
37mmΦ
28mmΦ
22mmΦ
17mmΦ
13mmΦ
10mmΦ
CNR
Acquition time(min)
0
25
50
75
100
1
5

(a) (b) (c)

Figure 9